



Supplementary Materials for

Exploring genetic suppression interactions on a global scale

Jolanda van Leeuwen, Carles Pons, Joseph C. Mellor, Takafumi N. Yamaguchi, Helena Friesen, John Koschwanez, Mojca Mattiazzi Ušaj, Maria Pechlaner, Mehmet Takar, Matej Ušaj, Benjamin VanderSluis, Kerry Andrusiak, Pritpal Bansal, Anastasia Baryshnikova, Claire Boone, Jessica Cao, Atina Cote, Marinella Gebbia, Gene Horecka, Ira Horecka, Elena Kuzmin, Nicole Legro, Wendy Liang, Natascha van Lieshout, Margaret McNee, Bryan-Joseph San Luis, Fatemeh Shaeri, Ermira Shuteriqi, Song Sun, Lu Yang, Ji-Young Youn, Michael Yuen, Michael Costanzo, Anne-Claude Gingras, Patrick Aloy, Chris Oostenbrink, Andrew Murray, Todd R. Graham, Chad L. Myers,* Brenda J. Andrews,* Frederick P. Roth,* Charles Boone*

*Corresponding author. Email: cmyers@cs.umn.edu (C.L.M.); brenda.andrews@utoronto.ca (B.J.A.); fritz.roth@utoronto.ca (F.P.R); charlie.boone@utoronto.ca (Ch.B.)

Published 4 November 2016, *Science* **354**, xxx (2016)
DOI: 10.1126/science.aag0839

This PDF file includes

Materials and Methods
Figs. S1 to S7
Captions for Tables S1 to S7
References

Other Supplementary Material for this manuscript includes the following:
(available at www.sciencemag.org/content/354/6312/aag0839/suppl/DC1)

Tables S1 to S7 as Excel files

Materials and Methods

Literature curation and statistical analysis

Literature curation

The *Saccharomyces cerevisiae* “synthetic rescue” dataset was downloaded from the BioGRID (9) on November 9, 2012 (version 3.1.49). Only interactions in which both interactors are yeast genes were considered. This dataset consisted of 4999 interactions described in 1564 papers. An additional 14 interactions were found and added while reading the papers. On March 31, 2014 version 3.2.110 of the dataset was downloaded from the BioGRID, and another 972 interactions were added, bringing the total to 5985 interactions described in 1667 papers. Each paper was read in detail, and an interaction was considered a suppression interaction if the double mutant grew significantly better than at least one of the single mutants. Suppressor and query alleles were annotated as deletion allele, hypomorphic allele (such as temperature sensitive (TS) and DAmP alleles), specific mutation (such as an activating or phosphorylation mutant), overexpression of a mutant allele, or spontaneous mutation if no further information was available. Notes were added for interactions that were identified under specific conditions (such as a drug or carbon source other than glucose, but not high temperature for TS alleles). Interactions that were not found in the paper, that were identified in a high-throughput study, that were not extragenic suppression interactions, in which a specific phenotype other than growth or survival was suppressed, that included more than two genes, or that suppressed a growth defect caused by overexpression of a gene, were removed from the dataset. In a few cases the interaction was annotated in the wrong direction, and suppressor and query were switched. The final dataset consisted of 1842 unique interactions, involving 1304 genes (Table S1).

Analysis of functional relatedness and overlap with other types of genetic interactions

We used several molecular and functional genome-scale datasets to evaluate the functional relatedness between suppression interaction pairs. We refer to these datasets as functional standards and they comprise GO term co-annotation, co-expression, co-localization, co-complex, and co-pathway relationships. In each case, only gene pairs for which functional data was available for both the query and the suppressor gene were considered. GO co-annotation was calculated only on biological process terms as previously described (6). The co-expression standard was derived from the MEFIT co-expression network, which integrates data from a collection of microarray experiments (48). Only gene pairs with a MEFIT score >1 were considered co-expressed. Co-localization relationships were calculated based on previously described localization data (49). Two genes whose products were found in at least one shared cellular compartment were defined as co-localized pairs. In the co-complex standard, which was described recently (6), gene pairs that were part of the same protein complex were considered as co-complexed, and gene pairs in distinct non-overlapping protein complexes were considered not co-complexed. The same approach was used to define the co-pathway standard using KEGG data (50).

For both the literature and systematic suppression interaction datasets we calculated the overlap with each of the functional standards. Significance of the overlap was assessed by Fisher's Exact tests. The expected overlap by chance was calculated by considering all possible pairs between a background set of queries and suppressors. The background set of queries consisted of genes found as queries in the suppression interaction dataset of interest. As background set of suppressors we considered all genes in the genome. Pairs in the suppression interaction dataset of interest were removed from the background set. For a given suppression interaction dataset and functional standard, we defined as fold enrichment the ratio between their overlap and the overlap of the background set of pairs with that standard.

For analysis of suppression interactions between and the distribution of genes over different biological processes, genes were assigned to broadly defined functional gene sets (2)(Table S7). Highly pleiotropic or poorly characterized genes were excluded from the analysis, as were functional categories to which only very few genes were assigned (e.g. “peroxisome” or “drug transport”). Significant enrichment was determined by Fisher's Exact test, comparing the observed to the expected proportion of genes in each functional category.

We compared our suppression interaction datasets to five different genetic networks: a dosage suppression interaction network (13) and four genetic interaction networks derived from a recent global genetic interaction dataset (6). By applying the standard cut-off to the global genetic network we defined the set of negative and positive genetic interactions, whereas by applying the stringent cut-off we defined the set of strong negative and positive genetic interactions (6). In the analyses involving the four genetic interaction networks, a single TS allele per essential gene was randomly selected and DAmP alleles were disregarded. Overlap of these genetic networks with the functional standards and with our suppression interaction datasets were calculated as explained above.

Yeast strains, plasmids, and growth assays

Yeast strains and plasmids

The suppressor strains are listed in Tables S2 and S6. All suppressor strains were part of either the BY4741 nonessential deletion mutant collection (*MATa xxxΔ::kanMX4 his3Δ1 leu2Δ0 ura3Δ0 met15Δ0*; Euroscarf), the SGA nonessential deletion mutant collection (*MATa xxxΔ::natMX4 can1Δ::Ste2pr-Sp_his5 lyp1Δ his3Δ1 leu2Δ0 ura3Δ0 met15Δ0*; (2)) or the corresponding *MATa* and *MATa* collections of DAmP or temperature sensitive mutants of essential genes (6). For suppressor confirmation experiments, the suppressor strains were crossed to the appropriate mutant strain of the opposite mating type from one these collections. For the plasmid complementation confirmation assays, plasmids from either the MoBY-ORF 2.0 (native promoter, *2μ*, *LEU2*, *kanMX4*; (13)) or the FLEX (*GAL1* promoter, *CEN/ARS*, *URA3*; (51)) collection were used. All other strains and plasmids used in this study are listed in Table S6.

Spot dilution assays and growth curves

Yeast strains were grown using standard rich (YPD) or minimal (SD) media. For spot dilution assays, strains were grown in selective media. Ten-fold serial dilutions were prepared by diluting cultures in water to optical densities (OD₆₀₀) of 0.1, 0.01, 0.001 and 0.0001. Five μ L aliquots were spotted onto agar plates and incubated at indicated temperatures. Plates were imaged after 48 h.

For papuamide A (University of British Columbia Depository) and duramycin (Sigma Aldrich) growth assays, saturated cultures were diluted to an OD₆₀₀ of 0.1, and seeded in 96-well plates at different drug concentrations. Plates were incubated at 34°C for 20 hours and the OD₆₀₀ was measured with a Multimode Plate Reader Synergy HT (Bio-Tek). Relative growth compared to vehicle-treated wild-type cells was calculated.

For oligomycin (Sigma Aldrich) growth assays, strains were grown overnight in YPD. The saturated cultures were diluted to an OD₆₀₀ of 0.1 in YPGly (1% w/v yeast extract, 2% w/v peptone, 3% v/v glycerol) and grown at 30°C. After 3h, 0-5 μ M oligomycin was added. Growth at 30°C was monitored continuously in an automated shaker and plater reader set-up (S&P robotics). Relative growth compared to wild-type cells treated with 1% DMSO was calculated.

Serial passaging

To construct deletion mutants expressing fluorescent proteins, *TEF2*-promoter driven E-GFP or tdtomato (RFP) were marked with *URA3* and integrated at the *ho* locus in Y7092, as previously described (5). The GFP and RFP strains were crossed with various strains from the *MATa xxx Δ ::kanMX4* deletion collection (Euroscarf) and SGA (18) was used to select *MATa xxx Δ ::kanMX4* strains with either *ho::TEF2pr-GFP::URA3* or *ho::TEF2pr-RFP::URA3*. Each strain was grown in triplicate to saturation in YPD, then equal OD units of wild type expressing GFP and mutant expressing RFP, as well as the reciprocal, were mixed in liquid and pinned from 96 to 768 format on two YPD + G418 (200 mg/L) plates. Plates were incubated at 30°C for 2 d, then one was imaged using a Typhoon fluorescence scanner with PMT 400 for GFP and 450 for RFP and the other was pinned to two YPD + G418 plates. This passaging was repeated five times for a total of six plates. Median fluorophore fluorescence for each colony was assessed using GenePix software as previously described (52). Unreliable values (<300 as determined from colonies of cells expressing no FP) were removed and values were normalized to the mean for each plate. The ratio of red:green or green:red was determined, and log₂ values of the means of each strain were plotted.

Similarly, fluorescently labeled W303 strains were created by integrating yeast enhanced Cerulean (CFP) or mCherry (RFP) into the *his3* locus of a W303 wild type or mutant strain. Strains were competed in liquid minimal media containing 80 mM glucose. Before each competition, the strains were individually grown to saturation, diluted, and then grown to log phase. The strains were then diluted and combined for the competitions. At eight time points, the cell concentration was measured on a Coulter counter, and fluorescence ratios were measured by FACS.

Systematic suppressor identification

Synthetic genetic array analysis

Synthetic genetic array (SGA) analysis was performed as described previously (6, 18). In short, in a typical SGA screen, a specific *natMX*-marked query mutation is crossed to an array of ~5000 *kanMX*-marked deletion mutants, and in a series of subsequent pinning steps haploid *natMX*- and *kanMX*-marked double mutants are selected. This not only generates a complete set of double mutants, it also represents a genome-wide set of two-factor crosses, which enables us to scan the query strain genome for the presence of an unmarked extragenic suppressor locus (20). When *kanMX*-marked deletion alleles derived from the array strains are positioned at a relatively short genetic distance from the suppressor mutation derived from the query strain, double mutant meiotic progeny carrying the *kanMX*-marked deletion tend not to carry the suppressor allele. Thus, for a collinear series of ~30 array genes in linkage with the suppressor locus, double-mutant colonies show a reduced size (20)(Fig. S3A). Similarly, *kanMX*-marked array strains carrying a suppressor mutation will yield smaller colonies when crossed into query strains for which the *natMX*-marked mutant allele is genetically linked to the suppressor locus. In total, we completed 7056 full-genome SGA screens involving mutant strains carrying deletion or hypomorphic alleles of 5845 different genes (2, 6).

Potential suppressor loci were detected automatically as follows: genetic interaction scores were calculated and sorted by chromosomal position of the array mutant. For each chromosome, the average, normalized standard deviation was calculated using the genetic interaction scores. Regions in which the rolling median genetic interaction score for 20 adjacent double mutants dropped below 80% of the negative chromosomal average standard deviation were subjected to visual inspection. This identified 251 strains that showed a potential suppressor linkage group in SGA (Tables S2 and S3).

Suppression magnitude

In SGA, single and double mutant fitness values are derived from normalized colony size measurements (6). A genetic interaction is defined using a multiplicative model, in which the genetic interaction score (ε) is the difference between the observed double mutant fitness (W_{QA}), and the multiplication of the query and array single mutant fitness ($W_Q \times W_A$).

$$\varepsilon = W_{QA} - W_Q \times W_A$$

In a screen using a query strain that carries a suppressor mutation, the measured fitness of the query and double mutants will actually be the fitness of the query and double mutants in presence of the suppressor (W_{QS} , W_{QAS}). The exception is within the suppressor linkage group, where the frequency of the suppressor allele will be low, and double mutant fitness will be representative of that in the absence of the suppressor (W_{QA}). Within each suppressor linkage group identified by SGA, we calculated the rolling median score for each set of 20 adjacent double mutants. We defined the lowest rolling median score within the suppressor linkage group as ε_{in} , and the median score amongst all double mutants on the array as ε_{out} . Using the multiplicative model to define a genetic interaction, the following equations are derived:

$$\epsilon_{\text{out}} = W_{\text{QAS}} - W_{\text{QS}} \times W_{\text{A}} \quad \text{and} \quad \epsilon_{\text{in}} = W_{\text{QA}} - W_{\text{QS}} \times W_{\text{A}}$$

As we are looking at averages over a large number of array mutants, and the deletion of most genes does not affect strain fitness, we assume the effect of the array deletion on the median scores is negligible ($W_{\text{QAS}} = W_{\text{QS}}$, $W_{\text{QA}} = W_{\text{Q}}$ and $W_{\text{A}} = 1$):

$$\epsilon_{\text{out}} = W_{\text{QS}} - W_{\text{QS}} = 0 \quad \text{and} \quad \epsilon_{\text{in}} = W_{\text{Q}} - W_{\text{QS}}$$

This gives an average ϵ_{out} of 0, consistent with most double mutants not showing a genetic interaction. The suppression magnitude is the difference between the fitness of a query with a suppressor and without the suppressor, thus:

$$\text{Suppression} = W_{\text{QS}} - W_{\text{Q}} = -\epsilon_{\text{in}}$$

A list of ϵ_{in} values (lowest rolling score within the suppressor linkage group) is available in Table S4.

Genetic validation of candidate suppressor genes

Each suppressor strain was subjected to three genetic crosses, followed by tetrad analysis of the meiotic progeny of the resulting diploid: 1) cross to a wild type strain to test for proper 2:2 segregation of the suppressor mutation, i.e. half of the spores carrying the query mutation are expected to show a fitness defect, while the other half are expected to be suppressed and have improved fitness. 2) Cross to a strain deleted for a gene genetically linked to a suppressor (“neighbor”) to test for proper linkage, i.e. all spores carrying both the query mutant and the neighbor deletion allele are expected to have a fitness defect, all spores carrying the query mutation but not the neighbor deletion are expected to be suppressed. 3) Cross to a strain carrying a deletion or conditional allele of the suppressor gene. If the suppressor mutation was a loss-of-function mutation, all spores carrying the query mutation are expected to be suppressed.

Additionally, the suppressor strains were transformed with plasmids carrying the wild-type allele of either the suppressor gene or of another gene within the suppressor linkage group. Either high-copy plasmids driving genes from their own promoter (13), or low-copy plasmids using the *GAL1*-promoter (51) were used. If the suppressor mutation is recessive or semi-dominant, overexpression of the wild type allele of the suppressor gene is expected to reverse the suppression and reduce the fitness of the suppressor strain. Each plasmid was transformed into a wild type strain as well, to make sure overexpression of the gene does not cause dosage lethality.

Lastly, we directly introduced 4 potential loss-of-function and 5 potential gain-of-function suppressor alleles into a diploid strain that was heterozygous for the corresponding query mutation. We amplified the genes carrying the suppressor mutation and a selection marker flanked by appropriate homology regions by PCR, and co-transformed the PCR-fragments into a diploid strain, in which one copy of the query gene was deleted. Proper integration of the mutated suppressor gene at its native locus was confirmed by PCR and Sanger sequencing. The diploids were sporulated and subjected to

tetrad analysis to determine whether the introduced mutations could suppress the growth defect of the query mutation. As a control, the wild type allele of the suppressor gene was introduced into the heterozygous diploid and subjected to tetrad analysis as well. Table S2 contains a summary of the results of each of these assays.

Sequencing and mutation calling

Sequencing, read mapping, and SNP and indel calling

Strains were sequenced on the Illumina HiSeq 2500 platform using paired-end 100-bp reads. Reads were aligned to the S288C reference genome from SGD (<http://yeastgenome.org>) using BWA (53) and SNPs and indels were identified using SAMtools (54). SNP/indels were called at stringent ($Q > 17$, read depth ≥ 10 , % high-quality bases supporting the alternate base ≥ 90 %) and permissive ($Q \geq 10$, read depth ≥ 3 , % high-quality bases supporting the alternate base > 50 %) thresholds. Structural variants (SVs) were detected using Pindel (Version - 0.2.4t)(55). A SV was called when insertions, deletions, and inversions were detected in 3 or more paired reads. Custom scripts were used to perform CNV and amino acid substitution analyses. To exclude pre-existing variants as well as systematic sequencing artifacts, variants were removed from consideration if they were present in at least 3 other sequenced strains (including the parental wild-type strain). Candidate suppressor mutations were confirmed by amplifying the corresponding gene and flanking sequences by PCR, followed by Sanger sequencing (Table S2). All whole-genome sequencing data is publicly available at NCBI's Sequencing Read Archive (<http://www.ncbi.nlm.nih.gov/sra>), under accession number SRP067030.

Identification of passenger mutations

For suppressor strains that were sequenced at a coverage of 10x or more, we defined passenger mutations as all SNPs and indels that were present in the strain, but not located in the query or in the suppressor gene (Table S5). We focused on SNPs and indels only, as SV calls had a high false positive rate. Passenger mutations were also identified in a control set of 72 strains that do not carry a suppressor mutation, but which were originally sequenced because they were suspected to carry the wrong query mutation. S375-392 were excluded from this analysis, as for these strains a slightly different pipeline was used to identify SNPs and indels. Recurrently mutated genes were defined as those that were mutated in at least 6 strains. 11 genes met this criteria, however, for 5 of those (*YNL338W*, *ASG1*, *YMR057W*, *HSM3*, *FLO9*), all mutations mapped to the same region of the gene, where either the read depth was low or the sequence was highly repetitive, suggesting they may be sequencing artifacts. For a subset of passenger mutations, the corresponding genes and flanking regions were amplified by PCR and sequenced using Sanger sequencing. The confirmation rate for the potential sequencing artifact genes was extremely low (0-10%), while the average confirmation rate for passenger mutations was ~75%, and thus we excluded these 5 genes from further analyses. Note that we do not expect a 100% confirmation rate using Sanger sequencing, as the passenger mutations may not be fixed in the strain.

Functional impact of suppressor and passenger mutations

The potential functional impact of suppressor and passenger mutations was assessed in four ways. 1) The fraction of mutations that occur in essential genes was calculated. 2) The deleteriousness of mutations was computed by SIFT (56), in which scores below 0.05 are predicted to be deleterious. 3) The fraction of mutations at protein-protein interaction interfaces was computed. For each protein for which a protein-protein complex structure was available in version 2015_05 of Interactome3D for *S. cerevisiae* (57), which is composed of experimental structures and complete homology models, we calculated the accessible solvent area (ASA) both when bound to the other protein(s) in the complex and in unbound form. We defined as interaction interface residues those showing a difference in ASA between the bound and unbound forms greater than 1 Å². Only mutations that could be mapped to a residue in a structure were considered. Mutations at an interaction interface are expected to have a relatively high functional impact. 4) The fraction of mutations that occur in disordered regions was calculated, by downloading disorder predictions by VSL2b (58) from D2P2 (59). Disordered regions allow a higher variability in sequence than structured regions, and mutations in disordered regions are thus expected to have a lower functional impact than those in structured regions. For each of these analyses only missense mutations were considered.

Importantly, we accounted for the possible bias introduced by suppressor and passenger genes for which multiple mutations were identified. In the protein-protein interface and disorder analyses, we randomly selected one mutation per gene and reported the median result across 1,000 randomizations. In the SIFT analysis, we computed the median SIFT score per gene.

Additional follow-up experiments

Mitochondrial F₁-ATP synthase protein structure

Crystal structure 2HLD (60) of the F₁-domain of the yeast mitochondrial ATP synthase was downloaded from the Protein Data Bank (<http://www.rcsb.org/pdb/>) and visualized using the PyMOL Molecular Graphics System, Version 1.4.1 Schrödinger, LLC.

Ymr010w topology

Ymr010w membrane topology was predicted using Phobius (61), and is in agreement with experimental data (62).

Fluorescence microscopy

Fluorescence microscopy was performed using a spinning-disc confocal (WaveFX, Quorum Technologies) connected to a DMI 6000B fluorescence microscope (Leica Microsystems) controlled by Velocity software (PerkinElmer), and equipped with an Imagem charge-coupled device camera (Hamamatsu C9100-13, Hamamatsu Photonics) and a 63x/NA1.4 Oil HCX PL APO objective. Yeast strains were grown to mid-log phase in appropriate selective synthetic media lacking tryptophan to minimize background fluorescence. All imaging was done at room temperature. 21 optical sections encompassing the whole cell were imaged at intervals of 0.3 μm. Images were processed using ImageJ (NIH, Bethesda, MD, USA; <http://imagej.nih.gov/ij/>).

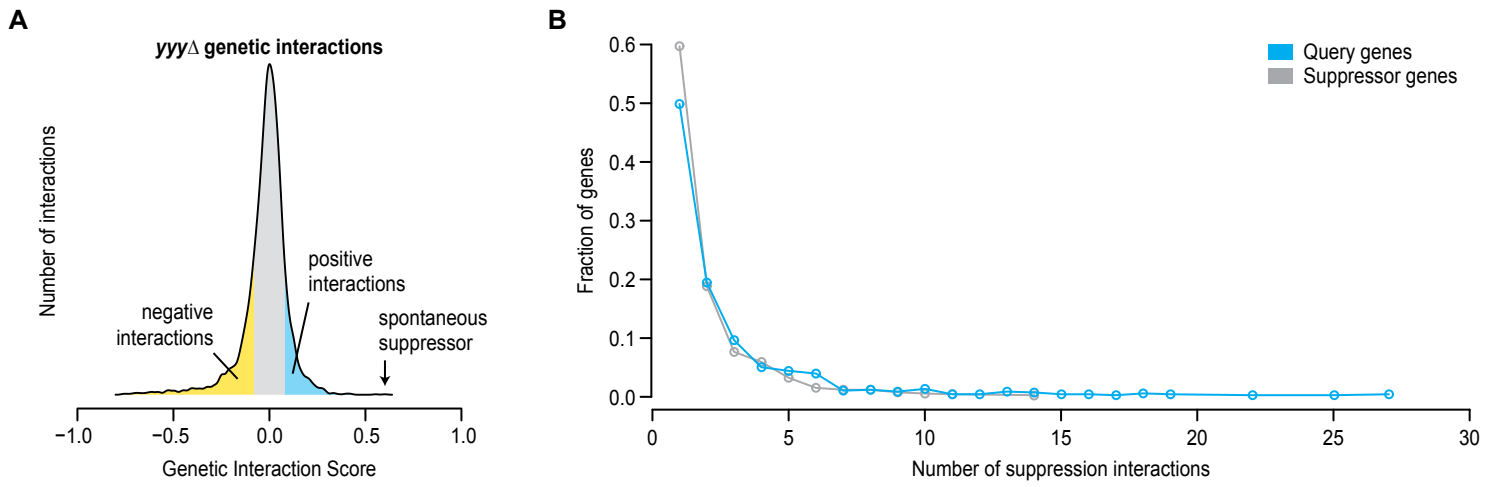


Fig. S1. Distribution of genetic interaction scores and suppression interaction degree. (A) Example of a distribution of genetic interactions of mutant *yyyΔ* determined by a genome-wide screen. The genetic interaction score is defined as the difference between the observed and the expected double mutant fitness (see Fig. 1A). Indicated are standard cut-offs for defining positive and negative interactions (2). Spontaneous suppressor mutations often represent the most extreme positive genetic interactions. (B) Degree distribution of suppression interactions. The number of suppression interactions was calculated for each query or suppressor in the set of 1842 suppression interactions curated from the biomedical literature (see Table S1). The number of suppression interactions was plotted against the fraction of query or suppressor genes showing that number of interactions.

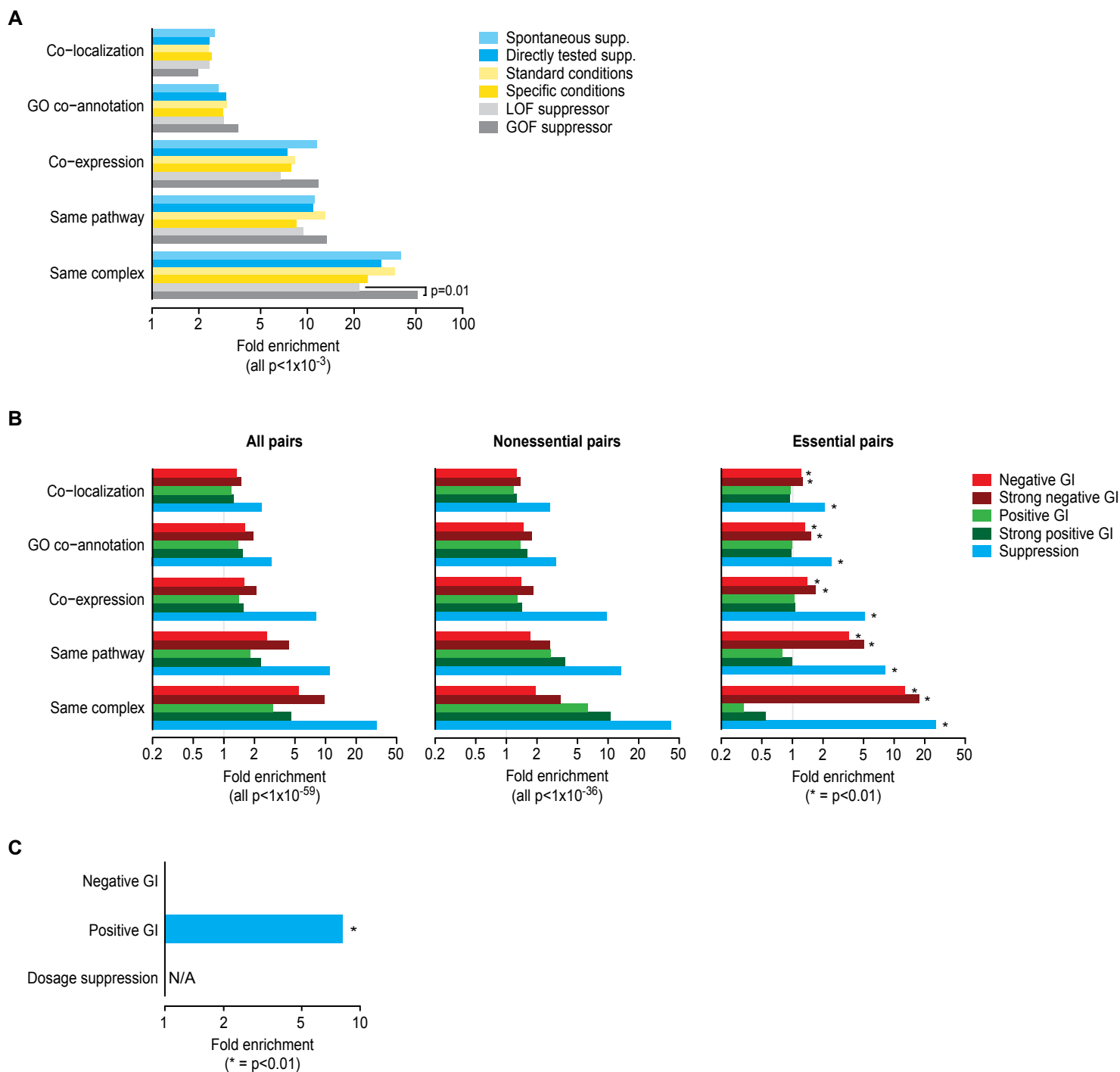


Fig. S2. Properties of genetic suppression interactions curated from literature. (A) Fold enrichment for co-localization, GO co-annotation, co-expression, same pathway membership, and same complex membership for different subsets of suppression interactions. Significance was determined using Fisher's Exact test. **(B)** Fold enrichments as in (A) are shown for gene pairs involved in different types of genetic interactions (GIs). Shown are the enrichments for all gene-pairs (left), pairs in which both genes are nonessential (middle), and pairs in which both genes are essential (right). Enrichments for positive and negative genetic interactions were calculated using either an intermediate or a stringent cut-off for scoring an interaction (2). **(C)** Fold enrichment for overlap of the literature-curated suppression interactions with negative genetic interactions, positive genetic interactions, or dosage suppression interactions considering only gene pairs for which deletion alleles were tested for suppression under standard laboratory conditions. None of the 45 suppression pairs that were tested for a genetic interaction in SGA showed a negative genetic interaction. The dosage suppression dataset only contains essential query genes.

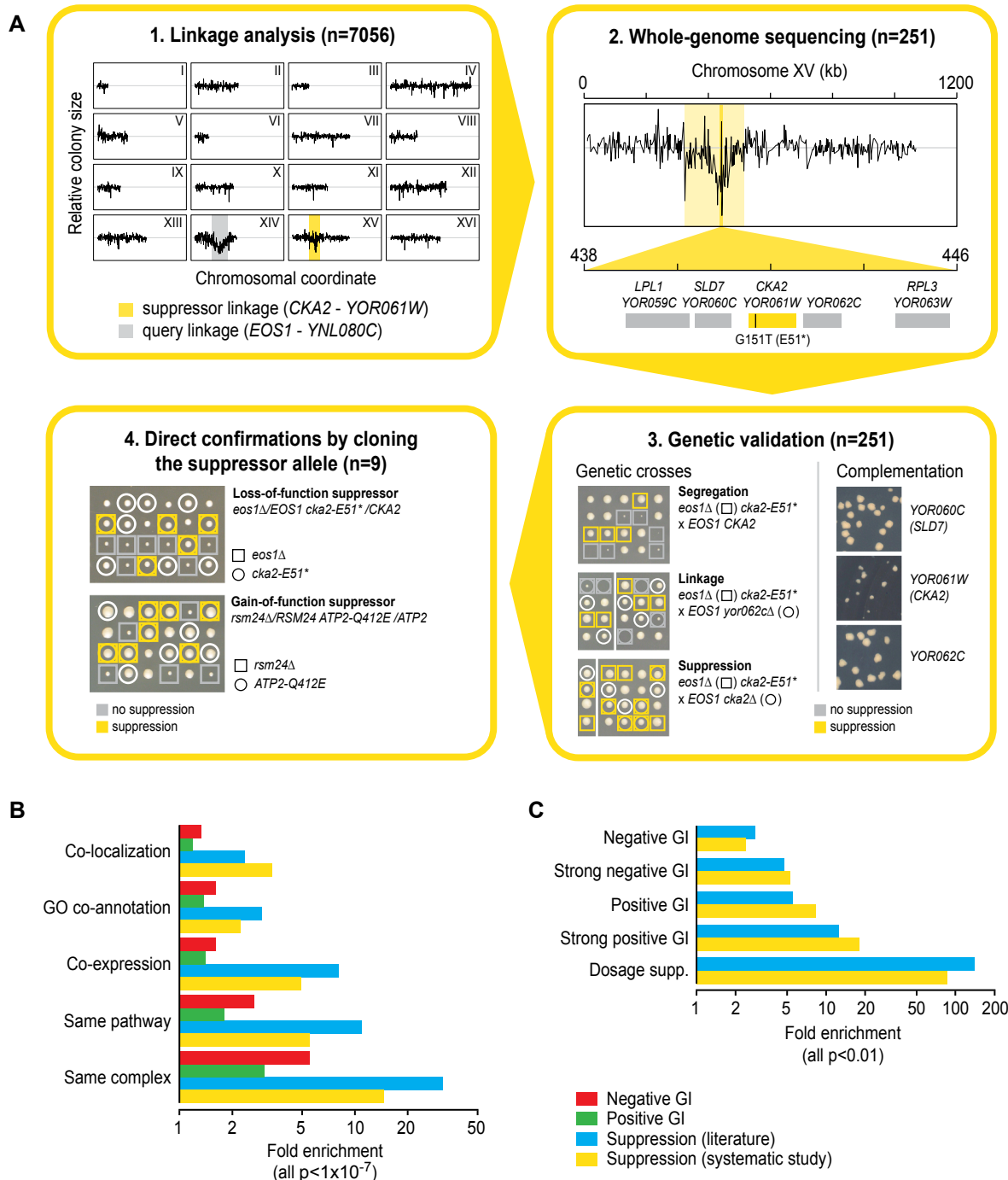


Fig. S3. Systematic identification of spontaneous suppressor mutations. (A) 1) 7056 strains containing different mutant alleles for 5845 ORFs were screened by Synthetic Genetic Array (SGA) analysis. For 251 of these strains (210 unique ORFs), SGA identified both the presence and the genomic location of a suppressor mutation by identifying a stretch of slow-growing colonies corresponding to mutants that have a genomic location in close proximity to the suppressor mutation. 2) Whole-genome sequencing of the suppressor strains was used to identify the suppressor mutation. 3) Suppression interactions were validated using several assays. First, the query strain carrying the suppressor mutation was crossed to a WT strain, a strain deleted for a gene linked to the suppressor, and a strain carrying a deletion or conditional allele of the suppressor gene, to determine proper segregation, linkage, and loss-of-function suppression, respectively. Next, the query strain carrying the suppressor mutation was transformed with a high-copy plasmid carrying the WT-allele of either the suppressor gene or a gene genetically linked to the suppressor, and growth was scored. 221 suppression interactions gave a positive result in at least one of the validation assays. 4) Finally, 9 suppressor genes were cloned directly into a strain heterozygous for the query mutation and sporulated. Tetrad analysis confirmed proper segregation of the suppression phenotype in all 9 cases. Table S2 contains a summary of the SGA, sequencing, complementation, and tetrad analysis results. (B, C) Comparison of literature and experimentally derived suppression interactions. Significance was determined using Fisher's Exact test. (B) Fold enrichment for co-localization, GO co-annotation, co-expression, same pathway membership, and same complex membership for gene pairs involved in different types of genetic interactions (GIs). (C) Fold enrichment for overlap with different types of genetic interactions for suppression gene pairs either identified by literature curation or experimentally-derived in this study. Enrichments for positive and negative genetic interactions were calculated using either an intermediate or a stringent cut-off for scoring an interaction (2).

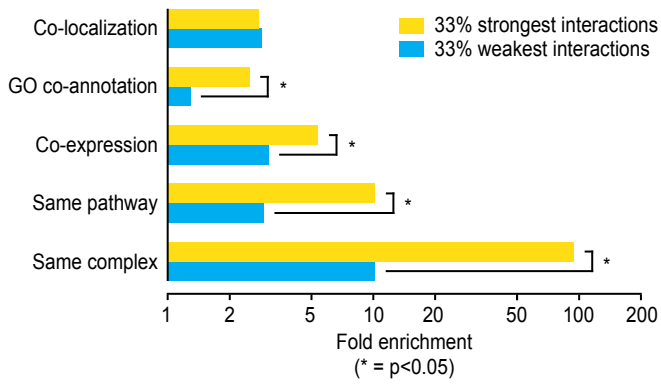


Fig. S4. Suppression magnitude correlates with functional relatedness. Suppression gene pairs identified by SGA mapping were ranked by suppression magnitude. In cases where the same interaction was identified more than once, the median score was calculated. For the strongest and weakest 33% of the suppression interactions, we computed the fold enrichment for gene pairs that were either annotated to the same GO-term, were co-expressed, or encoded proteins that co-localized or belonged to the same pathway or complex. Statistical significance was calculated using Fisher's Exact test.

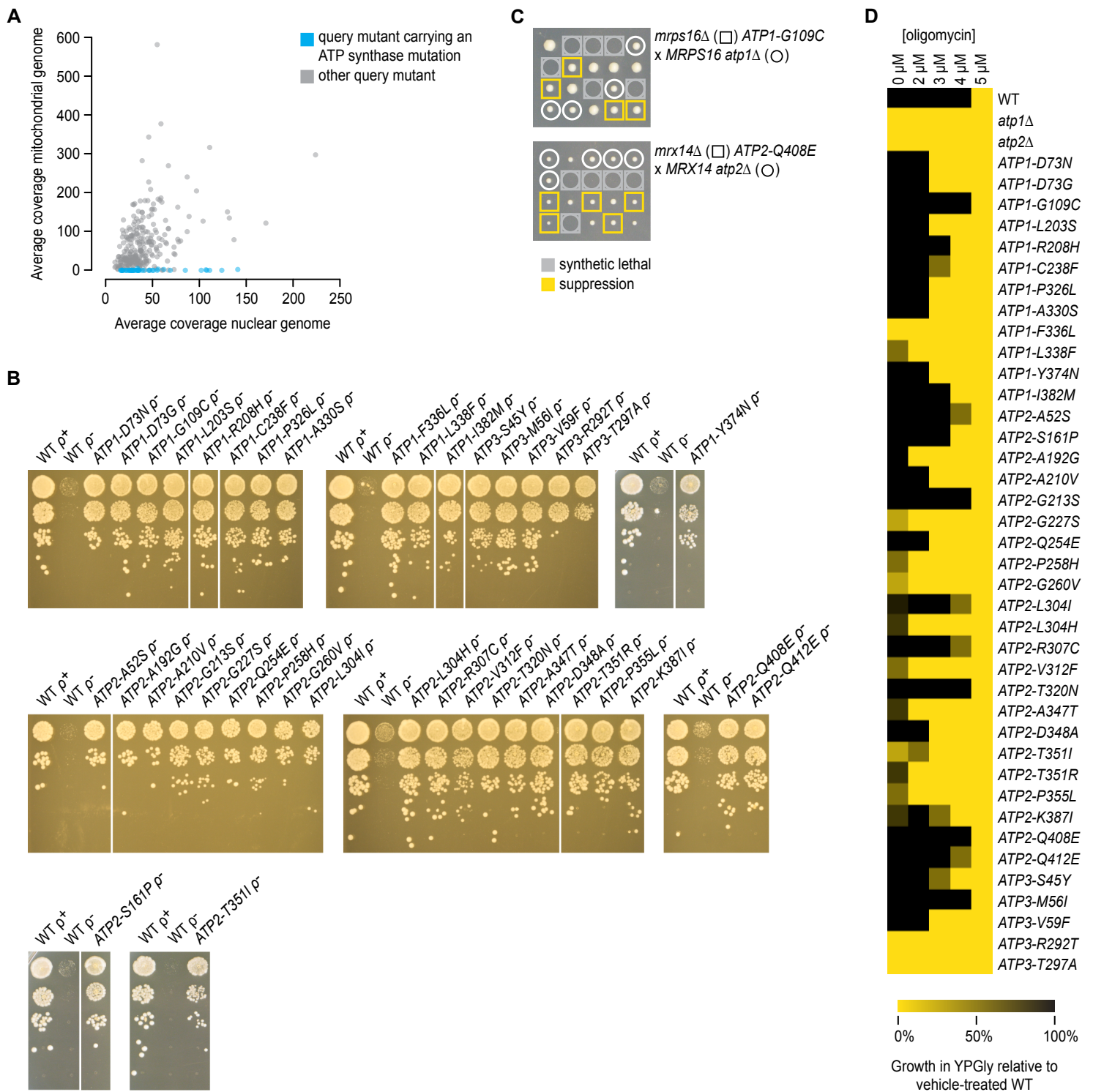


Fig. S5. Suppression of mitochondrial mutants by gain-of-function mutations in the F_1 -ATP synthase. (A) Query strains carrying ATP synthase mutations have lost their mitochondrial DNA. Average read depth of the nuclear and mitochondrial genomes as determined by whole-genome sequencing for strains either carrying a suppressor mutation in one of the mitochondrial ATP synthase subunits (blue), or not (grey). **(B)** ATP synthase-dependent suppression of slow growth caused by loss of the mitochondrial genome (ρ^-), in the absence of the query mutation. Exponentially growing cultures of the indicated strains were diluted to an optical density at 600 nm of 0.1 and a series of ten-fold dilutions was spotted on YPD agar plates and incubated at 30 °C for 2 days. **(C)** Loss of mitochondrial translation or transcription is synthetic lethal with deletion of *ATP1* or *ATP2*. Suppressor strains carrying both the query deletion in a gene involved in mitochondrial transcription or translation and a spontaneous suppressor mutation in either *ATP1* or *ATP2* were crossed to a strain deleted for the suppressor gene. The resulting diploids were sporulated and tetrads were dissected. **(D)** Suppressor mutations in the F_1 -ATP synthase decrease ATP synthesis activity. Growth profiles of ATP synthase mutants, in the absence of the query mutation, in YPGly media with different concentrations of oligomycin. Increased sensitivity to oligomycin is indicative of limited ATP production. Exponential growth of the mutants was scored relative to WT growth. Note that some mutants are unable to grow in YPGly media, even in the absence of oligomycin.

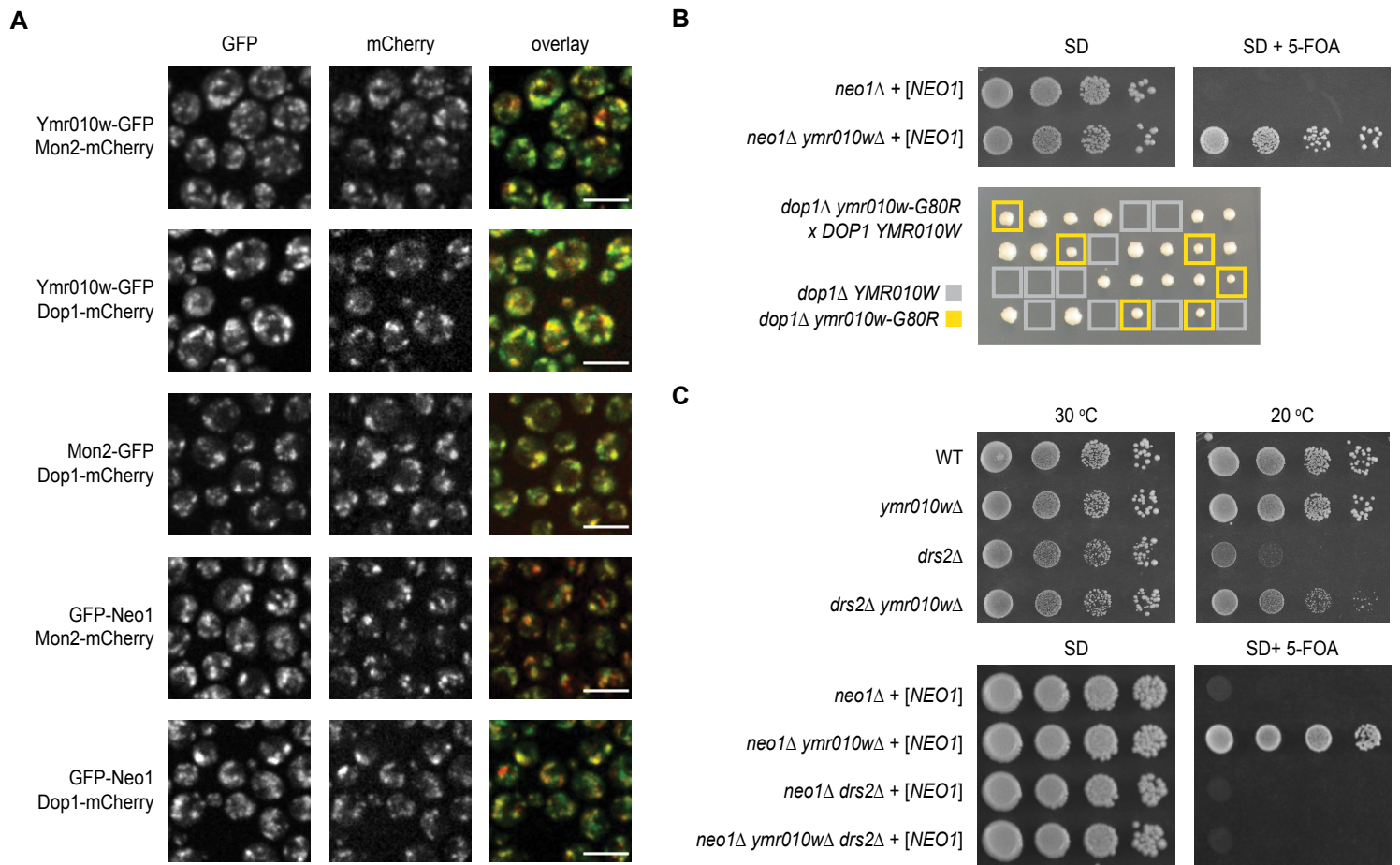


Fig. S6. Characterization of *YMR010W*. (A) Co-localization of Ymr010w with Mon2/Dop1/Neo1 complex members. Representative confocal brightfield and fluorescent micrographs of live, exponentially growing wild type cells with GFP or mCherry integrated at either the C-terminus of Mon2, Dop1, or Ymr010w, or the N-terminus of Neo1. Scale bar: 5 μ m. (B) Suppression of *neo1Δ* and *dop1Δ* lethality by mutation of *YMR010W*. Top: cultures of the indicated strains, all carrying a *URA3*-marked plasmid encoding *NEO1*, were diluted to an optical density at 600 nm of 0.1 and a series of ten-fold dilutions was spotted on agar plates and incubated at 27°C for 2d. Bottom: tetrad dissection analysis of a strain heterozygous for *dop1* and *ymr010w* mutant alleles. (C) Suppression of *drs2Δ* mutants. Spot dilutions as in (B) using the indicated strains.

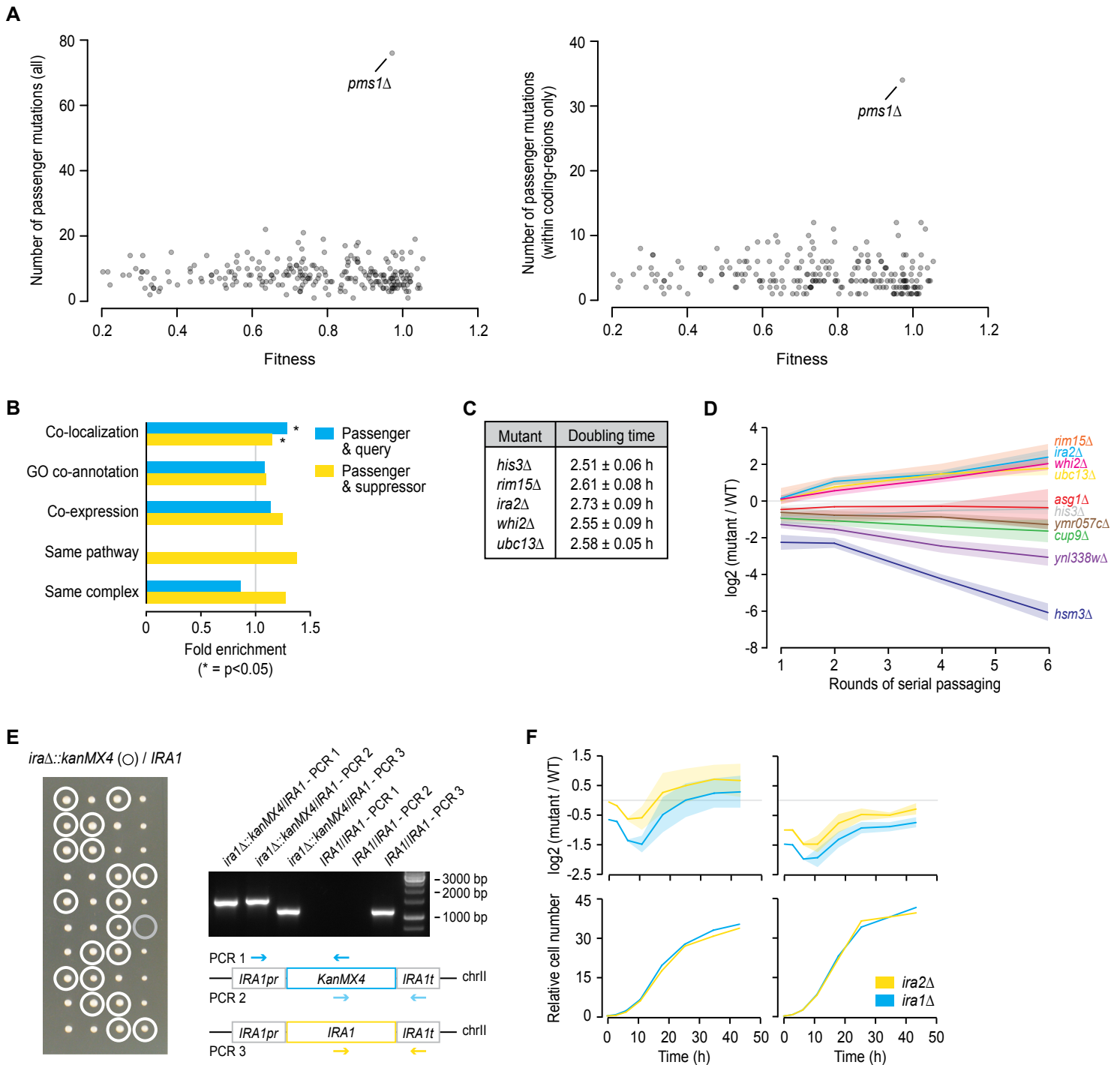


Fig. S7. Characterization of passenger mutations. (A) The relative fitness of a strain was plotted against the number of passenger mutations identified in the strain, either counting all passenger mutations (left), or counting only mutations that occurred within coding regions (right). Wild type fitness is normalized to 1.0. Passenger mutation and strain fitness data is available in Table S5. (B) Fold enrichment for co-localization, shared GO-annotation, co-expression, same pathway membership, and same complex membership for passenger and query or passenger and suppressor pairs. Significance was determined using Fisher's Exact test. None of the passenger and query pairs were members of the same pathway. (C) Average doubling times and standard deviations (SD) for the indicated mutant strains during exponential growth in YPD media at 30°C, n=6. (D) Differentially fluorescently labeled cells of the indicated mutants (GFP) and wild type (RFP) were mixed, spotted on agar plates, and the ratio of GFP to RFP was followed for 6 rounds of serial passaging. Shading represents the SD, n=12. Note that the RFP and GFP labels are reversed when compared to the data shown in Figure 5D. (E) Tetrad dissection and PCR confirmation of an *iraΔ::kanMX4/IRA1* heterozygous diploid S288c (BY4743) strain. Although deletion of *IRA1* is thought to be lethal in the S288c background, we were able to readily obtain viable *ira1Δ* haploid cells. (F) Differentially fluorescently labeled cells of the indicated mutants and wild type in the W303 background were mixed, and the ratio of the fluorophores was followed for 44h. Left: mutant-CFP and WT-RFP, right: mutant-RFP and WT-CFP. Shading represents the SD, n=3.

Table S1. Suppression interactions curated from the literature. The *S. cerevisiae* “synthetic rescue” data set was downloaded from the BioGRID, and further curated to solely include interactions in which the fitness defect caused by mutation of one gene was overcome by mutation of one other gene. The file lists the interactions that met our selection criteria (21), along with the corresponding BioGRID and PubMed IDs, the type of suppressor mutation (e.g., spontaneous mutation or deletion allele); the type of query mutation; and the use of specific conditions (e.g., a drug or specialized carbon source).

Table S2. Experimental suppression interactions identified by SGA. The suppression interactions that were identified experimentally by SGA analysis. It also contains details on the identification and confirmation of the suppressor mutations, including a summary of the results from SGA, sequencing, complementation assays, and tetrad analysis (21).

Table S3. SGA data of strains showing suppressor linkage groups. SGA scores for all suppressor strains, partitioned by mating type of the suppressor strain. Strains were either screened against an array of nonessential gene deletion mutants (FG) or an array of essential gene temperature-sensitive mutants (TS), at either 26° or 30°C. Please note that these data contain suppressor linkage groups that should be removed when scoring genetic interactions.

Table S4. Relative magnitude of the experimental suppression interactions. The relative magnitude of the experimental suppression interactions, measured as the lowest rolling scores within the suppressor linkage group identified by SGA (21). Strains were either screened against an array of nonessential gene deletion mutants (FG) or an array of essential gene temperature-sensitive mutants (TS), at either 26° or 30°C.

Table S5. Identified passenger mutations. A list of all identified passenger mutations for each sequenced yeast strain, as well as the average read depth and the normalized fitness of the strain.

Table S6. Yeast strains and plasmids. Details on all yeast strains and plasmids used in this study, and the source and/or lab from which they can be obtained.

Table S7. Functional categories for all yeast genes. Yeast genes that have been sufficiently characterized were assigned to 19 broadly defined functional gene sets (2). Highly pleiotropic genes were assigned to a separate category.

References and Notes

1. S. J. Dixon, M. Costanzo, A. Baryshnikova, B. Andrews, C. Boone, Systematic mapping of genetic interaction networks. *Annu. Rev. Genet.* **43**, 601–625 (2009). [Medline doi:10.1146/annurev.genet.39.073003.114751](#)
2. M. Costanzo, A. Baryshnikova, J. Bellay, Y. Kim, E. D. Spear, C. S. Sevier, H. Ding, J. L. Y. Koh, K. Toufighi, S. Mostafavi, J. Prinz, R. P. St Onge, B. VanderSluis, T. Makhnevych, F. J. Vizeacoumar, S. Alizadeh, S. Bahr, R. L. Brost, Y. Chen, M. Cokol, R. Deshpande, Z. Li, Z.-Y. Lin, W. Liang, M. Marback, J. Paw, B.-J. San Luis, E. Shuteriqi, A. H. Y. Tong, N. van Dyk, I. M. Wallace, J. A. Whitney, M. T. Weirauch, G. Zhong, H. Zhu, W. A. Houry, M. Brudno, S. Ragibizadeh, B. Papp, C. Pál, F. P. Roth, G. Giaever, C. Nislow, O. G. Troyanskaya, H. Bussey, G. D. Bader, A.-C. Gingras, Q. D. Morris, P. M. Kim, C. A. Kaiser, C. L. Myers, B. J. Andrews, C. Boone, The genetic landscape of a cell. *Science* **327**, 425–431 (2010). [Medline doi:10.1126/science.1180823](#)
3. R. Chen, L. Shi, J. Hakenberg, B. Naughton, P. Sklar, J. Zhang, H. Zhou, L. Tian, O. Prakash, M. Lemire, P. Sleiman, W. Y. Cheng, W. Chen, H. Shah, Y. Shen, M. Fromer, L. Omberg, M. A. Deardorff, E. Zackai, J. R. Bobe, E. Levin, T. J. Hudson, L. Groop, J. Wang, H. Hakonarson, A. Wojcicki, G. A. Diaz, L. Edelman, E. E. Schadt, S. H. Friend, Analysis of 589,306 genomes identifies individuals resilient to severe Mendelian childhood diseases. *Nat. Biotechnol.* **34**, 531–538 (2016). [Medline doi:10.1038/nbt.3514](#)
4. R. P. St Onge, R. Mani, J. Oh, M. Proctor, E. Fung, R. W. Davis, C. Nislow, F. P. Roth, G. Giaever, Systematic pathway analysis using high-resolution fitness profiling of combinatorial gene deletions. *Nat. Genet.* **39**, 199–206 (2007). [Medline doi:10.1038/ng1948](#)
5. D. K. Breslow, D. M. Cameron, S. R. Collins, M. Schuldiner, J. Stewart-Ornstein, H. W. Newman, S. Braun, H. D. Madhani, N. J. Krogan, J. S. Weissman, A comprehensive strategy enabling high-resolution functional analysis of the yeast genome. *Nat. Methods* **5**, 711–718 (2008). [Medline doi:10.1038/nmeth.1234](#)
6. M. Costanzo, B. VanderSluis, E. N. Koch, A. Baryshnikova, C. Pons, G. Tan, W. Wang, M. Usaj, J. Hanchard, S. D. Lee, V. Pelechano, E. B. Styles, M. Billmann, J. van Leeuwen, N. van Dyk, Z. Y. Lin, E. Kuzmin, J. Nelson, J. S. Piotrowski, T. Srikumar, S. Bahr, Y. Chen, R. Deshpande, C. F. Kurat, S. C. Li, Z. Li, M. M. Usaj, H. Okada, N. Pascoe, B. J. San Luis, S. Sharifpoor, E. Shuteriqi, S. W. Simpkins, J. Snider, H. G. Suresh, Y. Tan, H. Zhu, N. Malod-Dognin, V. Janjic, N. Przulj, O. G. Troyanskaya, I. Stagljjar, T. Xia, Y. Ohya, A. C. Gingras, B. Raught, M. Boutros, L. M. Steinmetz, C. L. Moore, A. P. Rosebrock, A. A. Caudy, C. L. Myers, B. Andrews, C. Boone, A global genetic interaction network maps a wiring diagram of cellular function. *Science* **353**, aaf1420 (2016). [10.1126/science.aaf1420 Medline doi:10.1126/science.aaf1420](#)
7. A. Baryshnikova, M. Costanzo, Y. Kim, H. Ding, J. Koh, K. Toufighi, J. Y. Youn, J. Ou, B. J. San Luis, S. Bandyopadhyay, M. Hibbs, D. Hess, A. C. Gingras, G. D. Bader, O. G. Troyanskaya, G. W. Brown, B. Andrews, C. Boone, C. L. Myers, Quantitative analysis of fitness and genetic interactions in yeast on a genome scale. *Nat. Methods* **7**, 1017–1024 (2010). [Medline doi:10.1038/nmeth.1534](#)

8. D. Botstein, *Decoding the Language of Genetics* (Cold Spring Harbor Laboratory Press, Cold Spring Harbor, New York, 2015).
9. C. Stark, B. J. Breitkreutz, T. Reguly, L. Boucher, A. Breitkreutz, M. Tyers, BioGRID: A general repository for interaction datasets. *Nucleic Acids Res.* **34**, D535–D539 (2006). [Medline doi:10.1093/nar/gkj109](#)
10. P. Shannon, A. Markiel, O. Ozier, N. S. Baliga, J. T. Wang, D. Ramage, N. Amin, B. Schwikowski, T. Ideker, Cytoscape: A software environment for integrated models of biomolecular interaction networks. *Genome Res.* **13**, 2498–2504 (2003). [Medline doi:10.1101/gr.1239303](#)
11. M. Valencia-Burton, M. Oki, J. Johnson, T. A. Seier, R. Kamakaka, J. E. Haber, Different mating-type-regulated genes affect the DNA repair defects of *Saccharomyces* RAD51, RAD52 and RAD55 mutants. *Genetics* **174**, 41–55 (2006). [Medline doi:10.1534/genetics.106.058685](#)
12. L. Peiró-Chova, F. Estruch, Specific defects in different transcription complexes compensate for the requirement of the negative cofactor 2 repressor in *Saccharomyces cerevisiae*. *Genetics* **176**, 125–138 (2007). [Medline doi:10.1534/genetics.106.066829](#)
13. L. Magtanong, C. H. Ho, S. L. Barker, W. Jiao, A. Baryshnikova, S. Bahr, A. M. Smith, L. E. Heisler, J. S. Choy, E. Kuzmin, K. Andrusiak, A. Kobylanski, Z. Li, M. Costanzo, M. A. Basrai, G. Giaever, C. Nislow, B. Andrews, C. Boone, Dosage suppression genetic interaction networks enhance functional wiring diagrams of the cell. *Nat. Biotechnol.* **29**, 505–511 (2011). [Medline doi:10.1038/nbt.1855](#)
14. E. L. Huttlin, L. Ting, R. J. Bruckner, F. Gebreab, M. P. Gygi, J. Szpyt, S. Tam, G. Zarraga, G. Colby, K. Baltier, R. Dong, V. Guarani, L. P. Vaites, A. Ordureau, R. Rad, B. K. Erickson, M. Wühr, J. Chick, B. Zhai, D. Kolippakkam, J. Mintseris, R. A. Obar, T. Harris, S. Artavanis-Tsakonas, M. E. Sowa, P. De Camilli, J. A. Paulo, J. W. Harper, S. P. Gygi, The BioPlex network: A systematic exploration of the human interactome. *Cell* **162**, 425–440 (2015). [Medline doi:10.1016/j.cell.2015.06.043](#)
15. T. Rolland, M. Taşan, B. Charlotiaux, S. J. Pevzner, Q. Zhong, N. Sahni, S. Yi, I. Lemmens, C. Fontanillo, R. Mosca, A. Kamburov, S. D. Ghiassian, X. Yang, L. Ghamsari, D. Balcha, B. E. Begg, P. Braun, M. Brehme, M. P. Broly, A. R. Carvunis, D. Convery-Zupan, R. Corominas, J. Coulombe-Huntington, E. Dann, M. Dreze, A. Dricot, C. Fan, E. Franzosa, F. Gebreab, B. J. Gutierrez, M. F. Hardy, M. Jin, S. Kang, R. Kiros, G. N. Lin, K. Luck, A. MacWilliams, J. Menche, R. R. Murray, A. Palagi, M. M. Poulin, X. Rambout, J. Rasla, P. Reichert, V. Romero, E. Ruyssinck, J. M. Sahalie, A. Scholz, A. A. Shah, A. Sharma, Y. Shen, K. Spirohn, S. Tam, A. O. Tejada, S. A. Trigg, J. C. Twizere, K. Vega, J. Walsh, M. E. Cusick, Y. Xia, A. L. Barabási, L. M. Iakoucheva, P. Aloy, J. De Las Rivas, J. Tavernier, M. A. Calderwood, D. E. Hill, T. Hao, F. P. Roth, M. Vidal, A proteome-scale map of the human interactome network. *Cell* **159**, 1212–1226 (2014). [Medline doi:10.1016/j.cell.2014.10.050](#)
16. R. Sopko, D. Huang, N. Preston, G. Chua, B. Papp, K. Kafadar, M. Snyder, S. G. Oliver, M. Cyert, T. R. Hughes, C. Boone, B. Andrews, Mapping pathways and phenotypes by systematic gene overexpression. *Mol. Cell* **21**, 319–330 (2006). [Medline doi:10.1016/j.molcel.2005.12.011](#)

17. M. E. Cusick, H. Yu, A. Smolyar, K. Venkatesan, A. R. Carvunis, N. Simonis, J. F. Rual, H. Borick, P. Braun, M. Dreze, J. Vandenhaute, M. Galli, J. Yazaki, D. E. Hill, J. R. Ecker, F. P. Roth, M. Vidal, Literature-curated protein interaction datasets. *Nat. Methods* **6**, 39–46 (2009). [Medline doi:10.1038/nmeth.1284](#)
18. A. H. Tong, M. Evangelista, A. B. Parsons, H. Xu, G. D. Bader, N. Pagé, M. Robinson, S. Raghizadeh, C. W. Hogue, H. Bussey, B. Andrews, M. Tyers, C. Boone, Systematic genetic analysis with ordered arrays of yeast deletion mutants. *Science* **294**, 2364–2368 (2001). [Medline doi:10.1126/science.1065810](#)
19. A. H. Tong, G. Lesage, G. D. Bader, H. Ding, H. Xu, X. Xin, J. Young, G. F. Berriz, R. L. Brost, M. Chang, Y. Chen, X. Cheng, G. Chua, H. Friesen, D. S. Goldberg, J. Haynes, C. Humphries, G. He, S. Hussein, L. Ke, N. Krogan, Z. Li, J. N. Levinson, H. Lu, P. Ménard, C. Munyana, A. B. Parsons, O. Ryan, R. Tonikian, T. Roberts, A. M. Sdicu, J. Shapiro, B. Sheikh, B. Suter, S. L. Wong, L. V. Zhang, H. Zhu, C. G. Burd, S. Munro, C. Sander, J. Rine, J. Greenblatt, M. Peter, A. Bretscher, G. Bell, F. P. Roth, G. W. Brown, B. Andrews, H. Bussey, C. Boone, Global mapping of the yeast genetic interaction network. *Science* **303**, 808–813 (2004). [Medline doi:10.1126/science.1091317](#)
20. P. Jorgensen, B. Nelson, M. D. Robinson, Y. Chen, B. Andrews, M. Tyers, C. Boone, High-resolution genetic mapping with ordered arrays of *Saccharomyces cerevisiae* deletion mutants. *Genetics* **162**, 1091–1099 (2002). [Medline](#)
21. Detailed materials and methods are available as supplementary materials in *Science* Online.
22. M. Schuldiner, S. R. Collins, N. J. Thompson, V. Denic, A. Bhamidipati, T. Punna, J. Ihmels, B. Andrews, C. Boone, J. F. Greenblatt, J. S. Weissman, N. J. Krogan, Exploration of the function and organization of the yeast early secretory pathway through an epistatic miniarray profile. *Cell* **123**, 507–519 (2005). [Medline doi:10.1016/j.cell.2005.08.031](#)
23. C. D. Dunn, R. E. Jensen, Suppression of a defect in mitochondrial protein import identifies cytosolic proteins required for viability of yeast cells lacking mitochondrial DNA. *Genetics* **165**, 35–45 (2003). [Medline](#)
24. G. D. Clark-Walker, Kinetic properties of F1-ATPase influence the ability of yeasts to grow in anoxia or absence of mtDNA. *Mitochondrion* **2**, 257–265 (2003). [Medline doi:10.1016/S1567-7249\(02\)00107-1](#)
25. A. Jézégou, E. Llinares, C. Anne, S. Kieffer-Jaquinod, S. O'Regan, J. Aupetit, A. Chabli, C. Sagné, C. Debacker, B. Chadeaux-Vekemans, A. Journet, B. André, B. Gasnier, Heptahelical protein PQLC2 is a lysosomal cationic amino acid exporter underlying the action of cysteamine in cystinosis therapy. *Proc. Natl. Acad. Sci. U.S.A.* **109**, E3434–E3443 (2012). [Medline doi:10.1073/pnas.1211198109](#)
26. A. K. Gillingham, J. R. Whyte, B. Panic, S. Munro, Mon2, a relative of large Arf exchange factors, recruits Dop1 to the Golgi apparatus. *J. Biol. Chem.* **281**, 2273–2280 (2006). [Medline doi:10.1074/jbc.M510176200](#)
27. S. Barbosa, D. Pratte, H. Schwarz, R. Pipkorn, B. Singer-Krüger, Oligomeric Dop1p is part of the endosomal Neolp-Ysl2p-Arl1p membrane remodeling complex. *Traffic* **11**, 1092–1106 (2010). [Medline doi:10.1111/j.1600-0854.2010.01079.x](#)

28. M. Takar, Y. Wu, T. R. Graham, The essential Neo1 protein from budding yeast plays a role in establishing aminophospholipid asymmetry of the plasma membrane. *J. Biol. Chem.* **291**, 15727–15739 (2016). [Medline doi:10.1074/jbc.M115.686253](#)
29. A. B. Parsons, A. Lopez, I. E. Givoni, D. E. Williams, C. A. Gray, J. Porter, G. Chua, R. Sopko, R. L. Brost, C. H. Ho, J. Wang, T. Ketela, C. Brenner, J. A. Brill, G. E. Fernandez, T. C. Lorenz, G. S. Payne, S. Ishihara, Y. Ohya, B. Andrews, T. R. Hughes, B. J. Frey, T. R. Graham, R. J. Andersen, C. Boone, Exploring the mode-of-action of bioactive compounds by chemical-genetic profiling in yeast. *Cell* **126**, 611–625 (2006). [Medline doi:10.1016/j.cell.2006.06.040](#)
30. K. Iwamoto, T. Hayakawa, M. Murate, A. Makino, K. Ito, T. Fujisawa, T. Kobayashi, Curvature-dependent recognition of ethanolamine phospholipids by duramycin and cinnamycin. *Biophys. J.* **93**, 1608–1619 (2007). [Medline doi:10.1529/biophysj.106.101584](#)
31. G. D. Fairn, M. Hermansson, P. Somerharju, S. Grinstein, Phosphatidylserine is polarized and required for proper Cdc42 localization and for development of cell polarity. *Nat. Cell Biol.* **13**, 1424–1430 (2011). [Medline doi:10.1038/ncb2351](#)
32. X. Teng, M. Dayhoff-Brannigan, W. C. Cheng, C. E. Gilbert, C. N. Sing, N. L. Diny, S. J. Wheelan, M. J. Dunham, J. D. Boeke, F. J. Pineda, J. M. Hardwick, Genome-wide consequences of deleting any single gene. *Mol. Cell* **52**, 485–494 (2013). [Medline doi:10.1016/j.molcel.2013.09.026](#)
33. G. I. Lang, D. P. Rice, M. J. Hickman, E. Sodergren, G. M. Weinstock, D. Botstein, M. M. Desai, Pervasive genetic hitchhiking and clonal interference in forty evolving yeast populations. *Nature* **500**, 571–574 (2013). [Medline doi:10.1038/nature12344](#)
34. S. Kryazhimskiy, D. P. Rice, E. R. Jerison, M. M. Desai, Global epistasis makes adaptation predictable despite sequence-level stochasticity. *Science* **344**, 1519–1522 (2014). [Medline doi:10.1126/science.1250939](#)
35. D. J. Kvittek, G. Sherlock, Whole genome, whole population sequencing reveals that loss of signaling networks is the major adaptive strategy in a constant environment. *PLOS Genet.* **9**, e1003972 (2013). [Medline doi:10.1371/journal.pgen.1003972](#)
36. E. Cameroni, N. Hulo, J. Roosen, J. Winderickx, C. De Virgilio, The novel yeast PAS kinase Rim 15 orchestrates G0-associated antioxidant defense mechanisms. *Cell Cycle* **3**, 462–468 (2004). [doi:10.4161/cc.3.4.791](#) [Medline](#)
37. A. Smith, M. P. Ward, S. Garrett, Yeast PKA represses Msn2p/Msn4p-dependent gene expression to regulate growth, stress response and glycogen accumulation. *EMBO J.* **17**, 3556–3564 (1998). [Medline doi:10.1093/emboj/17.13.3556](#)
38. D. Kaida, H. Yashiroda, A. Toh-e, Y. Kikuchi, Yeast Whi2 and Psr1-phosphatase form a complex and regulate STRE-mediated gene expression. *Genes Cells* **7**, 543–552 (2002). [Medline doi:10.1046/j.1365-2443.2002.00538.x](#)
39. K. Tanaka, M. Nakafuku, T. Satoh, M. S. Marshall, J. B. Gibbs, K. Matsumoto, Y. Kaziro, A. Toh-e, S. cerevisiae genes *IRA1* and *IRA2* encode proteins that may be functionally equivalent to mammalian *ras* GTPase activating protein. *Cell* **60**, 803–807 (1990). [Medline doi:10.1016/0092-8674\(90\)90094-U](#)

40. T. Hart, M. Chandrashekhar, M. Aregger, Z. Steinhart, K. R. Brown, G. MacLeod, M. Mis, M. Zimmermann, A. Fradet-Turcotte, S. Sun, P. Mero, P. Dirks, S. Sidhu, F. P. Roth, O. S. Rissland, D. Durocher, S. Angers, J. Moffat, High-resolution CRISPR screens reveal fitness genes and genotype-specific cancer liabilities. *Cell* **163**, 1515–1526 (2015). [Medline doi:10.1016/j.cell.2015.11.015](#)
41. T. Wang, K. Birsoy, N. W. Hughes, K. M. Krupczak, Y. Post, J. J. Wei, E. S. Lander, D. M. Sabatini, Identification and characterization of essential genes in the human genome. *Science* **350**, 1096–1101 (2015). [Medline doi:10.1126/science.aac7041](#)
42. V. A. Blomen, P. Májek, L. T. Jae, J. W. Bigenzahn, J. Nieuwenhuis, J. Staring, R. Sacco, F. R. van Diemen, N. Olk, A. Stukalov, C. Marceau, H. Janssen, J. E. Carette, K. L. Bennett, J. Colinge, G. Superti-Furga, T. R. Brummelkamp, Gene essentiality and synthetic lethality in haploid human cells. *Science* **350**, 1092–1096 (2015). [Medline doi:10.1126/science.aac7557](#)
43. E. M. Torres, T. Sokolsky, C. M. Tucker, L. Y. Chan, M. Boselli, M. J. Dunham, A. Amon, Effects of aneuploidy on cellular physiology and cell division in haploid yeast. *Science* **317**, 916–924 (2007). [Medline doi:10.1126/science.1142210](#)
44. A. B. Sunshine, C. Payen, G. T. Ong, I. Liachko, K. M. Tan, M. J. Dunham, The fitness consequences of aneuploidy are driven by condition-dependent gene effects. *PLOS Biol.* **13**, e1002155 (2015). [Medline doi:10.1371/journal.pbio.1002155](#)
45. L. M. Wahl, A. D. Zhu, Survival probability of beneficial mutations in bacterial batch culture. *Genetics* **200**, 309–320 (2015). [Medline doi:10.1534/genetics.114.172890](#)
46. C. M. Buchovecky, S. D. Turley, H. M. Brown, S. M. Kyle, J. G. McDonald, B. Liu, A. A. Pieper, W. Huang, D. M. Katz, D. W. Russell, J. Shendure, M. J. Justice, A suppressor screen in Mecp2 mutant mice implicates cholesterol metabolism in Rett syndrome. *Nat. Genet.* **45**, 1013–1020 (2013). [Medline doi:10.1038/ng.2714](#)
47. D. M. Jordan, S. G. Frangakis, C. Golzio, C. A. Cassa, J. Kurtzberg, E. E. Davis, S. R. Sunyaev, N. Katsanis; Task Force for Neonatal Genomics, Identification of cis-suppression of human disease mutations by comparative genomics. *Nature* **524**, 225–229 (2015). [Medline doi:10.1038/nature14497](#)
48. C. Huttenhower, M. Hibbs, C. Myers, O. G. Troyanskaya, A scalable method for integration and functional analysis of multiple microarray datasets. *Bioinformatics* **22**, 2890–2897 (2006). [Medline doi:10.1093/bioinformatics/btl492](#)
49. W. K. Huh, J. V. Falvo, L. C. Gerke, A. S. Carroll, R. W. Howson, J. S. Weissman, E. K. O’Shea, Global analysis of protein localization in budding yeast. *Nature* **425**, 686–691 (2003). [Medline doi:10.1038/nature02026](#)
50. M. Kanehisa, Y. Sato, M. Kawashima, M. Furumichi, M. Tanabe, KEGG as a reference resource for gene and protein annotation. *Nucleic Acids Res.* **44** (D1), D457–D462 (2016). [Medline doi:10.1093/nar/gkv1070](#)
51. Y. Hu, A. Rolfs, B. Bhullar, T. V. Murthy, C. Zhu, M. F. Berger, A. A. Camargo, F. Kelley, S. McCarron, D. Jepson, A. Richardson, J. Raphael, D. Moreira, E. Taycher, D. Zuo, S. Mohr, M. F. Kane, J. Williamson, A. Simpson, M. L. Bulyk, E. Harlow, G. Marsischky, R. D. Kolodner, J. LaBaer, Approaching a complete repository of sequence-verified

- protein-encoding clones for *Saccharomyces cerevisiae*. *Genome Res.* **17**, 536–543 (2007). [Medline doi:10.1101/gr.6037607](#)
52. P. Kainth, H. E. Sassi, L. Peña-Castillo, G. Chua, T. R. Hughes, B. Andrews, Comprehensive genetic analysis of transcription factor pathways using a dual reporter gene system in budding yeast. *Methods* **48**, 258–264 (2009). [Medline doi:10.1016/j.ymeth.2009.02.015](#)
 53. H. Li, R. Durbin, Fast and accurate short read alignment with Burrows-Wheeler transform. *Bioinformatics* **25**, 1754–1760 (2009). [Medline doi:10.1093/bioinformatics/btp324](#)
 54. H. Li, B. Handsaker, A. Wysoker, T. Fennell, J. Ruan, N. Homer, G. Marth, G. Abecasis, R. Durbin; 1000 Genome Project Data Processing Subgroup, The Sequence Alignment/Map format and SAMtools. *Bioinformatics* **25**, 2078–2079 (2009). [Medline doi:10.1093/bioinformatics/btp352](#)
 55. K. Ye, M. H. Schulz, Q. Long, R. Apweiler, Z. Ning, Pindel: A pattern growth approach to detect break points of large deletions and medium sized insertions from paired-end short reads. *Bioinformatics* **25**, 2865–2871 (2009). [Medline doi:10.1093/bioinformatics/btp394](#)
 56. R. Vaser, S. Adusumalli, S. N. Leng, M. Sikic, P. C. Ng, SIFT missense predictions for genomes. *Nat. Protoc.* **11**, 1–9 (2016). [Medline doi:10.1038/nprot.2015.123](#)
 57. R. Mosca, A. Céol, P. Aloy, Interactome3D: Adding structural details to protein networks. *Nat. Methods* **10**, 47–53 (2013). [Medline doi:10.1038/nmeth.2289](#)
 58. K. Peng, P. Radivojac, S. Vucetic, A. K. Dunker, Z. Obradovic, Length-dependent prediction of protein intrinsic disorder. *BMC Bioinformatics* **7**, 208 (2006). [Medline doi:10.1186/1471-2105-7-208](#)
 59. M. E. Oates, P. Romero, T. Ishida, M. Ghalwash, M. J. Mizianty, B. Xue, Z. Dosztányi, V. N. Uversky, Z. Obradovic, L. Kurgan, A. K. Dunker, J. Gough, D²P²: database of disordered protein predictions. *Nucleic Acids Res.* **41** (D1), D508–D516 (2013). [Medline doi:10.1093/nar/gks1226](#)
 60. V. Kabaleeswaran, N. Puri, J. E. Walker, A. G. Leslie, D. M. Mueller, Novel features of the rotary catalytic mechanism revealed in the structure of yeast F₁ ATPase. *EMBO J.* **25**, 5433–5442 (2006). [Medline doi:10.1038/sj.emboj.7601410](#)
 61. L. Käll, A. Krogh, E. L. Sonnhammer, A combined transmembrane topology and signal peptide prediction method. *J. Mol. Biol.* **338**, 1027–1036 (2004). [Medline doi:10.1016/j.jmb.2004.03.016](#)
 62. H. Kim, K. Melén, M. Osterberg, G. von Heijne, A global topology map of the *Saccharomyces cerevisiae* membrane proteome. *Proc. Natl. Acad. Sci. U.S.A.* **103**, 11142–11147 (2006). [Medline doi:10.1073/pnas.0604075103](#)